

Coverage dependence of oxygen decomposition and surface diffusion on rhodium (111): A DFT study

Oliver R. Inderwildi^{a)} and Dirk Lebedez

Interdisciplinary Center for Scientific Computing, University of Heidelberg, Im Neuenheimer Feld 368, 69120 Heidelberg, Germany

Olaf Deutschmann

Institute of Chemical Technology and Polymer Chemistry, University of Karlsruhe, Engesserstrasse 20, 76131 Karlsruhe, Germany

Jürgen Warnatz

Interdisciplinary Center for Scientific Computing, University of Heidelberg, Im Neuenheimer Feld 368, 69120 Heidelberg, Germany

(Received 8 June 2004; accepted 28 October 2004; published online 3 January 2005)

A systematic study of oxygen adsorption, decomposition and diffusion on Rh(111) and its dependence on coadsorbed oxygen molecules has been performed using density functional theory calculations. First, the bonding strength between metal surface and adsorbed oxygen molecules has been studied as a function of initial oxygen coverage. The bonding strength decreases with increasing oxygen coverage, which points towards a self-inhibition of the adsorption process. The potential energy hypersurface (PES) for the dissociation of oxygen molecules adsorbed on a threefold fcc position perpendicular to the surface was calculated using a combined linear/quadratic synchronous transit method with conjugate gradient refinements. The results indicate that a minor amount of oxygen on the surface enhances the decomposition of further oxygen molecules, while this process is inhibited at higher coverage. Moreover, PES calculations of a single site jump of atomic oxygen on rhodium (111) indicate that the activation energy increases as well with increasing oxygen coverage. All results are discussed with respect to a rhodium based catalytic NO_x reduction/decomposition system proposed by Nakatsuji, which decomposes nitrogen oxides in oxygen excess.

© 2005 American Institute of Physics. [DOI: 10.1063/1.1835891]

I. INTRODUCTION AND AIM

The purification of automotive exhaust gases is a widespread topic of academic and industrial research.^{1,2} For stoichiometrically operated engines ($\lambda \approx 1$), the well-known three-way catalyst is commonly used [the lambda oxidation value λ_{ox} is a measure for the ratio of oxidizing to reducing components in a gas mixture. Therefore, stoichiometric mixtures have a $\lambda_{\text{ox}} = 1$, oxygen rich mixtures have a $\lambda_{\text{ox}} > 1$ (lean) and oxygen depleted mixtures have a $\lambda_{\text{ox}} < 1$ (rich)]. The three-way catalyst oxidizes hydrocarbons (first way) as well as carbon monoxide (second way) and furthermore reduces NO_x ($x = 1, 2$) (third way) leading to near-zero emissions for these pollutants.³ This concept does not work for exhaust gases with higher oxygen concentrations (larger λ values). However, engines operated under the latter conditions became more popular recently, because of their higher fuel efficiency and consequently lower green house gas production. Furthermore, the amount of carbon monoxide and hydrocarbons emitted by these engines is negligible. However, a major disadvantage of this engine concept is that considerable amounts of nitrogen oxides are emitted and soot is formed. While it is a technically challenging task to

chemically reduce components in an oxygen rich environment, various concepts to decompose/reduce nitrogen oxides have been suggested.²

Most catalytic systems that fulfill these requirements suffer from the disadvantage of sulfur poisoning.⁴ Since attempts by the petroleum industry to reduce the sulfur concentration of fuels to near-zero values failed,⁵ concepts to reduce/decompose nitrogen in an oxygen-rich environment in the presence of sulfur compounds have to be developed. A new, promising route has been proposed by Nakatsuji and co-workers.^{6,7} Here, a supported rhodium catalyst is used to reduce NO_x under periodic oxygen-rich ($\lambda > 1$) and short oxygen depleted conditions ($\lambda < 1$). The NO_x reduction (short: DeNO_x) potential is high while the catalyst does not seem to deteriorate when sulfur-containing compounds are added. Nakatsuji proposed a mechanism for the surface processes involved, suggesting that during the oxygen depleted phase, the rhodium surface is reduced, while in the subsequent oxygen-rich phase the NO_x decomposes over the freshly reduced metal surface. It is known that in the absence of oxygen, NO decomposes over a reduced rhodium surface to initially form N₂⁶ leaving an oxidized rhodium surface that is inactive with respect to further NO decomposition.⁸

Since we consider exhaust gases with a minor amount of NO_x in a vast excess of oxygen, NO must consequently decompose much faster on the surface than oxygen. However,

^{a)}Electronic mail: inderwil@iwr.uni-heidelberg.de

kinetic investigations support the contrary.⁹ On this background, the process has been studied by means of density functional theory (DFT) calculations in order to investigate how the surface coverage influences the decomposition probability of oxygen on Rh(111). Since measuring these coverage dependencies experimentally is difficult, computational studies are a promising alternative to get a more detailed insight. Thermodynamic and kinetic properties of oxygen adsorption and decomposition have been studied as a function of the initial oxygen coverage.

DFT calculations are becoming a useful tool for estimating kinetic parameters for detailed surface reactions mechanisms. Nowadays, many microkinetic models are already based on elementary-step reaction mechanisms^{10,11} and such detailed models are increasing in number and popularity because of their higher accuracy and wide-ranging applicability compared to global kinetic models. This is mainly due to rate expressions, which do not depend on the external conditions, in contrast to those of global, over-all reactions. Therefore, models based on elementary-step reaction mechanisms can be extrapolated to a variety of different reaction conditions without any depletion in accuracy.^{11–13} This is especially interesting when conditions are explored that are difficult to investigate experimentally (e.g., extremely high temperatures, pressures or a combination of both).¹⁴ Moreover, especially the determination of the surface coverage dependencies of surface reactions by DFT methods is of general interest, because these are not easily accessible by conventional experimental techniques.

For a comprehensive modeling approach, in many cases the microkinetic models of heterogeneous as well as homogeneous chemical reactions are coupled to flow simulations. These combined models are then used to gain understanding and aid the development of technical processes such as the purification of exhaust gases.¹² The multiscale modeling can span length scales from angstrom to meters and time scales from microseconds to minutes/hours.¹⁵

II. METHODS

In the present work the reactions of oxygen on the surface of Rh(111) have been studied in DFT calculations using CASTEP (Cambridge Sequential Total Energy Package).¹⁶ The generalized gradient approximation (GGA) as proposed by Perdew and Wang¹⁷ was applied combined with Vanderbilt ultrasoft pseudopotentials.¹⁸ Where necessary, spin effects have been taken into account by using the spin polarized (dependent) GGA functional (GGSA). The plane wave basis set was truncated at a kinetic energy of 300 eV. Computations were performed over a range of k points within the Brillouin zone as generated by the Monkhorst-Pack scheme.¹⁹ The preciseness of the Monkhorst-Pack scheme was chosen so that the k -point spacing is similar for all investigated unit cells.

The surface was modeled as a rhodium slab with the thickness of three atomic layers. Periodic-boundary conditions extrapolate from a metal cluster to an extended surface. Various publications show that the thickness of three layers is sufficient to generate a model of a transition metal surface,

exemplarily we refer to a study by Nørskov and co-workers.²⁰

Location and extent of the elementary cell for the DFT calculations were chosen in a way to obtain the desired surface coverage. A 10 Å vacuum was placed in between the periodic slabs to ensure that adsorbate and subsequent slab do not interact. The positions of the metal atoms were fixed in (111) surface configuration, while the positions of the adsorbates were fully mobile. To determine the adsorption energies ΔE_{ads} , the target surface was geometry optimized with the oxygen molecule added on the one hand and without the oxygen molecule on the other hand; the energies of the optimized surfaces were calculated subsequent to the geometry optimization. The geometry of the oxygen molecule was optimized within a cell similar to the cell of the surface and the energy of this optimized oxygen crystal E_{O_2} was calculated subsequently. Finally the adsorption energies were determined according to

$$\Delta E_{ads} = E_{slab+O_2} - (E_{slab} + E_{O_2}). \quad (1)$$

The structures of reactants and products were relaxed prior to calculating activation energies as well as reaction heats for the oxygen dissociation. The transition state of the reaction was located on the potential energy hypersurface (PES) by performing a linear synchronous combined with a quadratic synchronous transit calculation and conjugate gradient refinements.²¹ The total energies for reactants, transition state, and products were computed. Heats of reaction were calculated according to

$$\Delta E_{reaction} = E_{products} - E_{reactants} \quad (2)$$

and the activation energy was then calculated according to

$$E_{act} = E_{transition\ state} - E_{reactants} \quad (3)$$

Mulliken charges were calculated according to a formalism described by Segall *et al.*²²

III. RESULTS AND DISCUSSIONS

A. Clean rhodium and molecular oxygen

In a preliminary calculation we optimized the geometry of bulk rhodium. A lattice constant of 3.804 Å was detected which is in good agreement with the experimentally determined value of 3.803 Å.²³ Furthermore, this result is similar to former DFT-GGA calculations.^{24,25}

Molecular oxygen was optimized using the DFT-GGSA functional. The bond length of free triplet ground state O₂ was calculated to be 1.21 Å [expt: 1.21 Å (Ref. 26)]. When oxygen is placed in a supercell corresponding to that used in the subsequent chapter, the bond length increases to 1.23 Å. Both lengths indicate an oxygen-oxygen double bond.

B. Molecular oxygen on Rh(111)

A situation with oxygen adsorbed perpendicularly to the metal surface (end-on) in a threefold (fcc) position on top of a Rh(111) with (2×2) periodicity has been the starting point of our study. Walter *et al.* showed that there is indeed a stable molecular oxygen species adsorbed on rhodium (111) which is nonparamagnetic in high coordination sites (hcp- as well

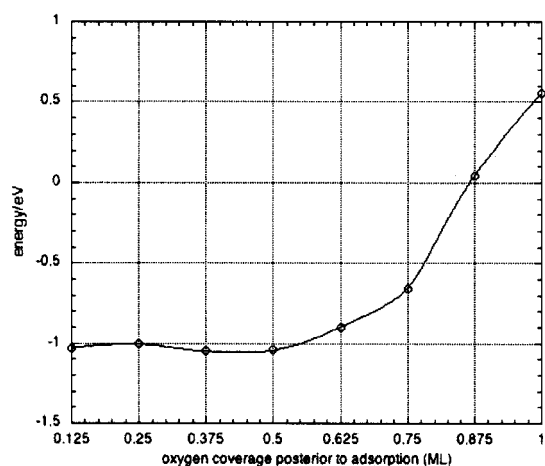


FIG. 1. Heat of adsorption as a function of the initial oxygen coverage.

as fcc-threefold position).²⁷ Our structure optimizations and energetic calculations confirm that there is a stable, nonparamagnetic end-on adsorbed molecular oxygen state on a fcc-threefold site as well.²⁸ The oxygen atom pointing towards the surface is located 1.51 Å above it. Rhodium-oxygen distances are calculated to be 2.17 Å; the oxygen-oxygen distance is 1.33 Å according to our calculation.

In a first step, the dependence of the strength of the oxygen bonding on the oxygen coverage of the rhodium (2×4) surface has been studied by calculating the heat of adsorption according to 1. It could be shown that the bonding of molecular oxygen to the rhodium surface becomes weak at high oxygen coverages, these results are in accordance with a study carried out by Ganduglia-Pirovano *et al.*²⁵ for atomic oxygen. The heat of adsorption as a function of the initial surface coverage is depicted in Fig. 1.

It indicates that a minor initial oxygen coverage of the rhodium surface enhances the adsorption of further oxygen molecules while the process is inhibited at higher coverages and even blocked at coverages close to 1 ML. This effect might be electronically induced. The electronegative oxygen withdraws electrons from the metal surface and hence lowers the back-donation effect of the metal into the antibonding π orbital of the adsorbed molecular oxygen species. This effect is hindered when further oxygen withdraws electrons from the metal surface.

The suggested weaker back-donation effect is supported by bond length analysis. The O–O bond length of the adsorbed molecular oxygen decreases from 1.31 Å ($\theta=0.125$) to 1.26 Å ($\theta=1$), indicating a higher bond order of the oxygen molecule. To determine whether the origin of this effect is indeed electronic, charge analysis of the end-on adsorbed species were carried out.

1. Mulliken charge analysis of the end-on adsorbed oxygen molecule

In order to verify if the decrease in adsorption energy is due to a weaker electron donation, Mulliken charge analysis of the end-on adsorbed O₂ molecule with different oxygen preoccupations was performed. The results show that the electronic donation from the rhodium surface to the adsorbed molecular species decreases with increasing oxygen preoccupa-

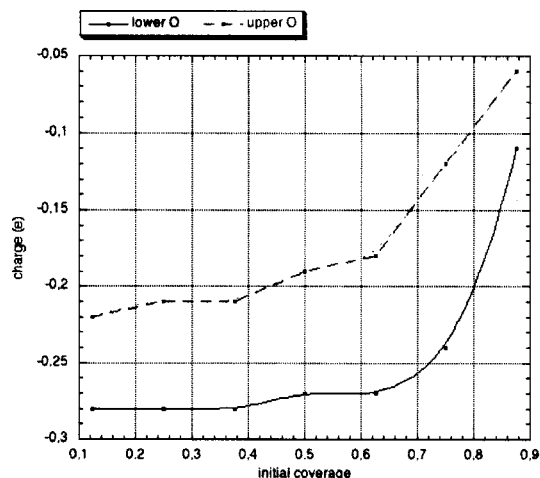


FIG. 2. Mulliken charges of oxygen atoms of the end-on adsorbed oxygen molecule as function of the initial oxygen coverage. Lower oxygen refers to the oxygen atom bonded to the rhodium surface.

tion. As can be seen in Fig. 2, the partial charges on the upper as well as the lower oxygen atom of the end-on adsorbed species decrease with increasing oxygen preoccupation. The weaker electron donation from the rhodium surface to the adsorbed molecule supports the decrease in adsorption energy calculated. Moreover, the charge analysis results are in agreement with the calculated bond length of the end-on adsorbed oxygen molecule. The contraction of the oxygen-oxygen bond with increasing oxygen preoccupation indicates a higher bond order, which is due to decreasing electron donation into the antibonding orbital as supported by Mulliken charge analysis.

Moreover, we point out that the shapes of the coverage functions of the partial charges are similar to the shape of the coverage function of the adsorption energy, indicating that this effect is indeed electronically induced.

To conclude, the decreasing adsorption energy calculated could support the mechanism proposed by Nakatsuji (see Introduction), because the oxygen coverage would possibly stagnate at a certain coverage. The effect may favor the adsorption and decomposition of nitrogen oxides and hence provide further insight into the functioning of the NO_x decomposition catalyst.

C. Atomic oxygen on rhodium (111)

The optimal geometry of atomic oxygen adsorbed in a threefold-fcc position on Rh(111) has been studied. In accordance with LEED studies and DFT calculations our geometry optimisations allow the conclusion that atomic oxygen preferably resides in threefold positions on the rhodium surface.²⁵

At a surface coverage of $\theta=0.25$ [2 O-(2×2)/Rh(111)] the optimal distance for an atomic oxygen in fcc position was calculated to be 1.296 Å above the rhodium surface, well in agreement with low energy electron diffraction (LEED) studies [$1.24 \text{ Å} \pm 0.06 \text{ Å}$ (Ref. 29)] as well as DFT calculations carried out by Ganduglia-Pirovano *et al.*²⁵ The rhodium oxygen distance was calculated to be 2.02 Å (LEED: $2.00 \text{ Å} \pm 0.08 \text{ Å}$) and the Rh-Rh interlayer spacing

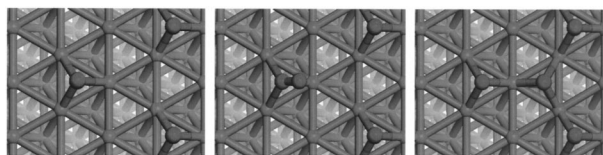


FIG. 3. Adsorbed oxygen molecule, decomposition transition state, and decomposed oxygen on (2×2)-rhodium (111).

was calculated to be 2.23 Å again very well in accordance with experimental data [LEED: 2.24 Å±0.04 Å (Ref. 29)] and former DFT studies.²⁵ For atomic oxygen in a threefold-hcp position distances are only slightly different, the oxygen is located 1.29 Å above the rhodium surface in this model and the Rh–O distance was calculated to be 2.01 Å.

D. Decomposition process

It is known that end-on adsorbed diatomic molecules preferably decompose with the breaking bond coordinated over a single metal atom rather than coordinated over a surface metal-metal bond.³⁰ Furthermore, they decompose in a fashion that after decomposition the surface atoms share the smallest number of surface metal atoms possible (principle of least atom sharing).³¹ Based on this knowledge, a preferred final conformation of the dissociated molecule was assumed as depicted in Fig. 3 (right).

Since atomic species are much more sensitive towards changes in surface configuration than molecular species (see the adsorption energies against surface coordination number in Table I), the energy of reaction strongly depends on the topology of the decomposed molecule rather than on the topology of the adsorbed molecule.

Figure 3 shows the computed optimal topologies for end-on adsorbed oxygen as well as its decomposition products. The computed transition state for the decomposition is also depicted and it can be seen that first the oxygen-oxygen bond has to bend into the direction of the decomposing metal atom and in the transition state the oxygen atoms are still bonded to each other, while both are bonded to the decomposing rhodium atom. From the transition state (maximum energy point along the reaction coordinate), the oxygen atom simply “drops” into its preferred adsorption site, meaning that the process is going energetically strictly downhill as expected.

Placing additional atomic oxygen atoms [initial coverage (θ_{init})=0.5] on top of the rhodium surface, and recalculating the optimal geometries (starting materials/products) a determination of the transition state as described in Sec. II shows

TABLE I. Influence of the surface coordination numbers onto the heat of adsorption of end-on adsorbed molecular oxygen and atomic oxygen.

Coordination number	O ₂ (eV)	O (eV)
1	−0.06	0.01
2	−0.38	−0.99
3	−0.50	−1.12

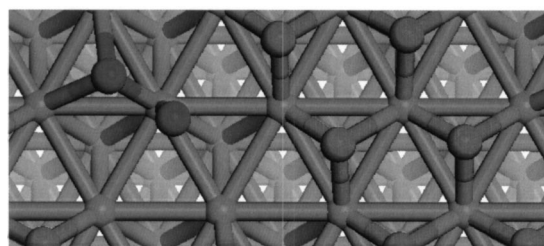


FIG. 4. The transition state of the oxygen decomposition (left, marked by color/shade) at an initial oxygen coverage of 0.625.

that the additional oxygen inhibits further decomposition of oxygen molecules, even though the decomposition is sterically still unhindered.

To investigate this effect in more detail, a surface with a (2×4) elementary cell consisting of eight surface rhodium atoms has been modeled in order to vary the initial oxygen coverage over a broader range. The atomic coordinates of the metal atoms have been constrained so that the 111 facet is conserved while the adsorbates were assumed to be mobile. Only for high coverages ($\theta \geq 0.75$) constraints were imposed on the adsorbates, so that a vacant surface site adjacent to the oxygen molecule is available to ensure geometrically unhindered decomposition. The geometries for the oxygen molecule as well as its decomposition products have been calculated for different oxygen coverages. The transition state of the reaction of the molecule to its decomposition products was determined for different initial oxygen coverages. As an example, the transition state of the oxygen decomposition at an initial oxygen coverage of $\theta_{\text{init}}=0.625$ is shown in Fig. 4. The activation energies as well as the reaction energies have been calculated according to formulas (2) and (3).

It could be shown that for increasing oxygen coverage, the activation energy of the oxygen decomposition increases (Fig. 5) while the reaction gets less exothermic (Fig. 6). Only for small initial oxygen coverages the activation energy decreases, suggesting a doping effect. For surface coverages above $\theta_{\text{init}}=0.25$ the activation energy of the decomposition process increases almost exponentially.

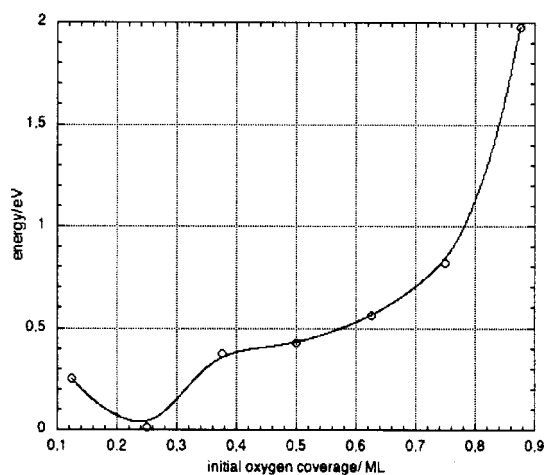


FIG. 5. Activation energy of the oxygen decomposition as a function of the initial oxygen surface coverage.

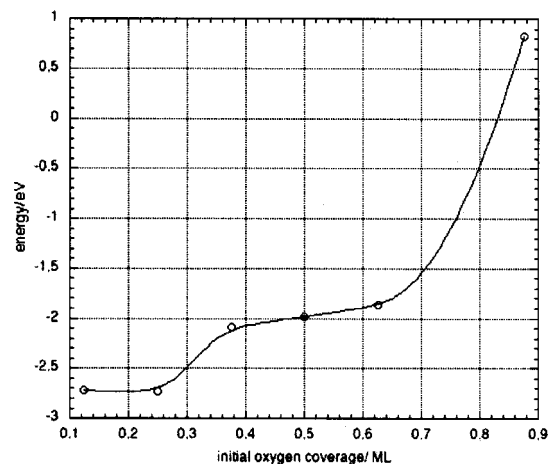


FIG. 6. Coverage dependence of the reaction energies of the oxygen decomposition.

Furthermore, the heat of reaction of oxygen decomposition decreases with increasing initial coverage. At coverages close to a monolayer the reaction is even endothermic, see Fig. 5. [Preliminary calculations of the decomposition at high oxygen coverages using a five layer rhodium slab support the results (E_a and $\Delta E_{\text{reaction}}$) found with the three layer rhodium slab. This indicates that the results are not an artifact of the used model.]

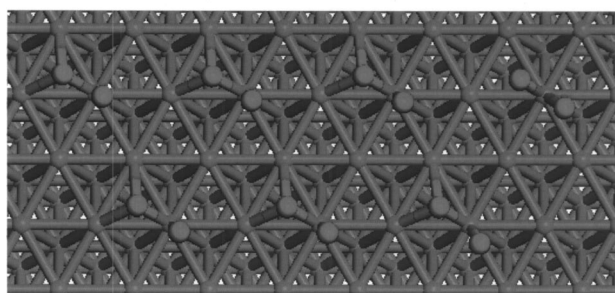
This observation as well points towards a strong inhibition of the oxygen decomposition at medium initial oxygen coverages as already observed by temperature programmed desorption (TPD) experiments.³²

To determine the origin of this effect, charge, and geometry analysis of the transition states were carried out.

1. Analysis of the transition state geometries

Analysis of the geometry of the calculated transition states for the oxygen decomposition on Rh(111) surfaces shows that the position of the transition state depends on the oxygen preoccupation. The location of the transition state shifts in the reaction coordinate towards the product geometry. For clarity the transition states of the oxygen decompo-

$\theta_{\text{INIT}} = 0.125$ $\theta_{\text{INIT}} = 0.375$ $\theta_{\text{INIT}} = 0.625$ $\theta_{\text{INIT}} = 0.875$



$\theta_{\text{INIT}} = 0.25$ $\theta_{\text{INIT}} = 0.5$ $\theta_{\text{INIT}} = 0.75$

FIG. 7. Transition states of the oxygen decomposition with increasing oxygen preoccupation. For the sake of clarity, the oxygen preoccupation is not shown.

TABLE II. Exact geometries of the different transition state structures. For atom numbering please see Fig. 8. ϵ denotes the angle by which the oxygen atoms is tilted out of the surface normal plane (depicted in Fig. 8, bottom), positive angle denotes tilting towards Rh² and Rh⁵, negative angle in towards Rh¹ and Rh⁴; α denotes the angle between lower O, Rh³, and upper O (see Fig. 8, top).

θ_{init}	Lower O				Upper O				α (deg) (O–Rh–O)
	Distance to (Å)				Distance to (Å)				
	Rh ¹	Rh ²	Rh ³	ϵ (deg)	Rh ³	Rh ⁴	Rh ⁵	ϵ (deg)	
0.125	2.15	2.15	1.99	0.00	1.97	3.17	3.18	-0.58	51.6
0.250	2.17	2.13	1.99	0.97	1.93	3.08	3.00	2.48	56.3
0.375	2.18	2.12	1.97	1.57	1.93	3.15	3.07	2.83	53.4
0.500	2.20	2.13	1.97	1.66	1.92	3.01	2.99	3.54	55.2
0.625	2.20	2.22	1.97	-0.29	1.93	3.08	2.77	1.12	54.2
0.750	2.19	2.19	1.97	-0.23	2.00	2.96	2.59	11.91	52.9
0.875	2.49	2.53	1.99	-0.87	2.13	2.81	2.77	1.12	55.4

sition on (2×4)-Rh(111) without oxygen preoccupation ($\theta_{\text{init}}=0.125$) and with different amounts of oxygen preoccupation ($\theta_{\text{init}}=0.25-0.875$) are depicted in Fig. 7.

The oxygen atoms in the transition state of the oxygen decomposition get closer to their positions in the product structures with increasing oxygen preoccupation. In the transition state for the oxygen decomposition leading to a complete monolayer of oxygen (see Fig. 7, top right) the oxygen atoms are 1.92 Å apart while they are rather close to their positions in the product structure (threefold fcc as well as hcp). Thus, the transition states calculated and heats of reactions obtained from these calculations are in well accordance with Hammond's postulate.

Hammond's postulate states that the transition state of an exothermic reaction occurs early in the reaction coordinate (reactantlike transition state), while it occurs late in the reaction coordinate for endothermic reactions (productlike transition state).³³

The geometries of the different transition states are given in Table II.

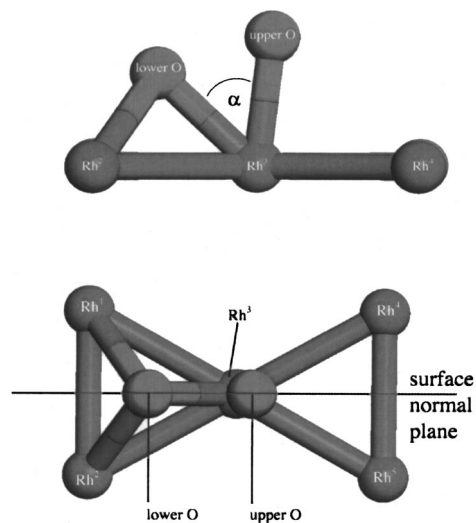


FIG. 8. Example transition state with atom numbering, surface normal plane, and oxygen-rhodium-oxygen angle α .

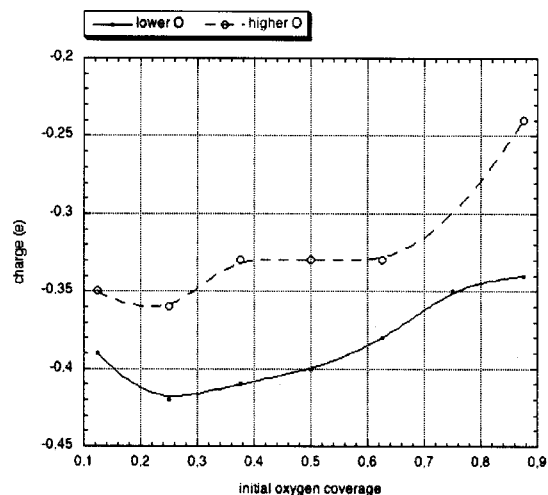


FIG. 9. Mulliken charges of the oxygen atoms in the transition state of the oxygen decomposition. Lower oxygen refers to the oxygen atom bonded to the rhodium surface in the reactant structure.

The described increase in activation energy might be due to the electron withdrawing effect of the adsorbed oxygen. As discussed in Sec. III B the electronegative oxygen withdraws electrons from the metal surface and hence lowers the back-donation effect of the metal into the antibonding π orbital of the adsorbed molecular oxygen species. This effect is hindered when further oxygen withdraws electrons from the metal atom, as supported by charge analysis (see Sec. III B). To verify if this electron withdrawing effect is also the reason for the alteration of activation barrier, Mulliken charge analysis of the transition state structures were performed.

2. Mulliken charge analysis of the transition state of the oxygen decomposition

Charge analysis of the transition states have shown that at low oxygen coverage (0.25 ML) electron donation from the surface to the oxygen atoms is more pronounced than without oxygen preoccupation. This indicates a stabilization of the transition state for 0.25 ML oxygen coverage and hence can explain the lowered activation barrier for the decomposition. For higher coverages the partial charges of the

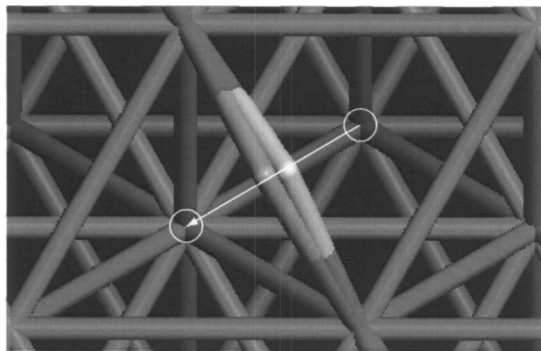


FIG. 10. On top view of the transition states of an oxygen single site jump at different coverages on rhodium (111) from a fcc- to a hcp-threefold position (white circles) along the reaction coordinate (white arrow). Transition states of this process for coverages of 0.25 ML (ML—monolayer) (light gray) and 0.5 ML (dark gray) are depicted.

TABLE III. Transition states geometries; for atom numbering see Fig. 11.

θ	Distances of O to (\AA)				β (deg)	h (\AA) (Surface-O)
	Rh ¹	Rh ²	Rh ³	Rh ⁴		
0.25	2.77	1.90	1.89	2.60	90.6	1.40
0.50	2.76	1.97	1.91	2.68	87.6	1.33

oxygen atoms decrease which indicates a destabilization of the transition state. This leads to an increase of the activation energies calculated for surface coverages higher than 0.3 ML. As in the case of oxygen adsorption, also here, the shape of the graphs of the partial charges of the oxygen atoms and the graph of the activation energy are similar indicating a direct correlation (Fig. 9).

E. Oxygen single site jump and surface diffusion

In order to learn more about the microscopic details of the behavior of oxygen on rhodium (111), the PES for a single site jump of atomic oxygen from a fcc threefold position (Fig. 10, white circle) to an adjacent hcp-threefold position (Fig. 10, gray circle) was calculated. This calculation was carried out for oxygen coverages of 0.5 ML [O-(1 \times 2)-Rh(111)] as well as 0.25 ML [O-(2 \times 2)-Rh(111)]. Also in this case, the surface diffusion process seems to be coverage dependent. As intuitively expected, the transition state of the single site jump is located in the region of the bridged species between the two threefold positions. The activation energy of the surface jump process is calculated to be 0.47 eV at 0.25 ML, while 0.57 eV at 0.5 ML. In both cases it is endothermic, with an energy change of 0.08 eV and 0.1 eV for 0.25 ML and 0.5 ML, respectively. Analysis of the transition state geometry shows that the calculated thermodynamic and kinetic data are in accordance with Hammond's postulate, since the transition state of the stronger endothermic reaction (Fig. 10, dark gray atom) is located later along the reaction coordinate (Fig. 10, white arrow) than the more exothermic (Fig. 10, light gray atom).

Furthermore, Mulliken charge analysis of the transition states was carried out to verify if the origin of the increase of the activation barrier is electronical. The partial charge of the oxygen atom in the transition state is $-0.51e$ in case of 0.25 ML (Fig. 10, light gray atom), while it is only $-0.47e$ in case of 0.5 ML (Fig. 10, dark gray atom). This indicates a stronger stabilization of the transition state in the case of the

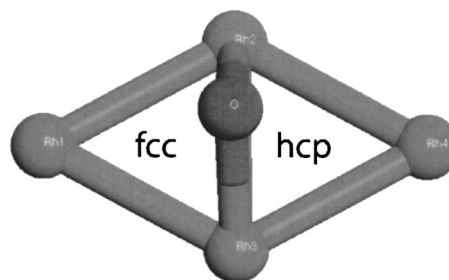


FIG. 11. Example transition state for an oxygen single site jump with atom numbering.

lower coverage and hence supports the assumption that the origin of the investigated effect is indeed electronical.

Exact geometries of the transition states structures are given in Table III.

IV. CONCLUSIONS

DFT calculations show that oxygen coverage of the rhodium (111) surface weakens the bonding of the oxygen molecule to the rhodium surface. This surmises that with increasing oxygen coverage the adsorption probability of O₂ decreases, oxygen decomposition therefore gets statistically more unlikely and hence the oxygen coverage stagnates. Moreover, the study shows that there is a stable end-on adsorbed molecular oxygen species on rhodium (111), however, the calculated energy barrier-towards the decomposed oxygen is rather low, pointing towards a rather fast decomposition.

A minor extent of oxygen preoccupation on a rhodium surface even enhances the ability of rhodium to decompose molecular oxygen. However, at higher initial oxygen coverages, this ability is obstructed, supporting the suggestion that oxygen coverage stagnates. As can be seen in Fig. 5, on the right-hand side of the minimum for the activation energy at $\theta=0.25$ the activation energy increases almost exponentially. Since the decomposition process is sterically unhindered (an unoccupied surface site next to the adsorbed oxygen molecule is kept vacant), this increase in activation energy is most likely due to the electron withdrawing effect of the oxygen. This hypothesis is supported by Mulliken charge analysis.

Moreover, the energy of reaction of the oxygen decomposition becomes smaller with increasing surface coverage. At high surface coverages ($\theta_{\text{init}}=0.875$) the decomposition reaction is even endothermic, which again points towards a stagnation of the oxygen decomposition at medium oxygen coverages. Transition state analysis supports the calculated decrease in exothermicity, because this decrease is in agreement with Hammond's postulate. All these theoretical results are in accordance with TPD experiments.³²

The conclusions drawn from this study support the surface mechanism proposed by Nakatsuji and co-workers.⁶ The decrease in oxygen decomposition activity of rhodium surface with increasing oxygen coverage up to a stagnation of the process could explain the NO decomposition activity at high oxygen concentrations. Nitrogen oxide in a vast excess of oxygen could still decompose over rhodium even though the initial kinetics support the contrary, since the kinetics are coverage dependent. The oxygen decomposition is very likely at low coverages while it gets improbable for higher oxygen coverages. Therefore, the NO_x decomposition activity of rhodium could be attributed to partially oxidized rhodium surfaces.

Moreover, this study shows that DFT calculations are a powerful tool with respect to the quantitative determination of coverage dependencies of kinetic parameters. Since these are difficult to determine experimentally, DFT calculations are a tool that can fill this gap and can hence aid the development of elementary step surface reaction mechanisms.

The results from this study will provide the basis for kinetic modelling of the transient surface process to investigate the catalytic properties on a realistic scale.³⁴

ACKNOWLEDGMENTS

The presented work was partially supported by German Federal Ministry of Education and Research via the ConNeCat network and by the German Research Foundation via the collaborative research center "Reactive Flows, Diffusion, and Transport." The authors would like to thank the members of the ConNeCat-consortium "Automotive Exhaust Gas Aftertreatment" for advice and guidance and Dr. J. Piechota (ICM, Warsaw University) as well as Dr. A. Sundermann (hte AG, Heidelberg) for fruitful discussions.

- ¹G. C. Koltsakis and A. M. Stamatelos, *Prog. Energy Combust. Sci.* **23**, 1 (1997); T. Kreuzer, E. S. Lox, D. Lindner, and J. Leyrer, *Catal. Today* **29**, 17 (1996).
- ²L. S. Glebov, A. G. Zakirova, V. F. Tret'yakov, T. N. Burdeinaya, and G. S. Akopova, *Petroleum Chemistry (Neftekhimiya)*, ISSN: 0965-5441 **42**, 143 (2002).
- ³R. M. Heck and R. J. Farrauto, *Appl. Catal., A* **221**, 443 (2001).
- ⁴A. Amberntsson, E. Fridell, and M. Skoglundh, *Appl. Catal., B* **46**, 429 (2003).
- ⁵C. Song, *Catal. Today* **86**, 211 (2003).
- ⁶T. Nakatsuji and V. Komppa, *Appl. Catal., B* **30**, 209 (2001).
- ⁷T. Nakatsuji and V. Komppa, *Catal. Today* **75**, 407 (2002).
- ⁸K. Almusateer, R. Krishnamurthy, and S. S. C. Chuang, *Catal. Today* **55**, 291 (2000).
- ⁹C. S. Gopinath and F. Zaera, *J. Catal.* **200**, 270 (2001).
- ¹⁰O. Deutschmann, *Chem.-Ing.-Tech.* **72**, 987 (2000).
- ¹¹D. K. Zerkle, M. D. Allendorf, M. Wolf, and O. Deutschmann, *J. Catal.* **196**, 18 (2000).
- ¹²D. Chatterjee, O. Deutschmann, and J. Warnatz, *Faraday Discuss.* **119**, 371 (2001).
- ¹³O. Deutschmann and L. D. Schmidt, *AIChE J.* **44**, 2465 (1998); O. Deutschmann, R. Schmidt, F. Behrendt, and J. Warnatz, *Proc. Combust. Inst.* **26**, 1747 (1996); O. Deutschmann, R. Schwiedernoch, L. I. Maier, and D. Chatterjee, in *Natural Gas Conversion VI*, Studies in Surface Science and Catalysis Vol. 136, edited by E. Iglesia, J. J. Spivey, and T. H. Fleisch (Elsevier, Amsterdam, 2001), p. 251; L. D. Schmidt, O. Deutschmann, and J. C. T. Goralski, *Modeling the Partial Oxidation of Methane to Syngas at Millisecond Contact Times* (Elsevier, Amsterdam, 1998).
- ¹⁴O. Deutschmann, U. Riedel, and J. Warnatz, *Proceedings of the Second European Symposium on Aerothermodynamics for Space Vehicles*, ESA SP-367, pg. 305, 1995.
- ¹⁵S. Tischer, C. Correa, and O. Deutschmann, *Catal. Today* **69**, 57 (2001); R. Schwiedernoch, S. Tischer, C. Correa, and O. Deutschmann, *Chem. Eng. Sci.* **58**, 633 (2003); J. Windmann, J. Braun, P. Zacke, D. Chatterjee, O. Deutschmann, and J. Warnatz, *SAE Tech. Pap. Ser. I*, 0937 (2003).
- ¹⁶M. D. Segall, P. L. D. Lindan, M. J. Probert, C. J. Pickard, P. J. Hasnip, S. J. Clark, and M. C. Payne, *J. Phys.: Condens. Matter* **14**, 2717 (2002).
- ¹⁷J. P. Perdew, J. A. Chevary, S. H. Vosko, K. A. Jackson, M. R. Pederson, and C. Fiolhais, *Phys. Rev. B* **46**, 6671 (1992).
- ¹⁸D. Vanderbilt, *Phys. Rev. B* **41**, 7892 (1990).
- ¹⁹H. J. Monkhorst and J. D. Pack, *Phys. Rev. B* **13**, 5188 (1976).
- ²⁰M. Mavrikakis, J. Rempel, J. Greeley, L. B. Hansen, and J. K. Nørskov, *J. Chem. Phys.* **117**, 6737 (2002).
- ²¹N. Govind, M. Petersen, G. Fitzgerald, D. King-Smith, and J. Andzelm, *Comput. Mater. Sci.* **28**, 250 (2003).
- ²²M. D. Segall, R. Shah, C. J. Pickard, and M. C. Payne, *Phys. Rev. B* **54**, 16317 (1996).
- ²³C. Kittel, *Introduction to Solid State Physics*, 6th ed. (Wiley, New York, 1986); P. Villars and L. D. Calvert, *Pearson's Handbook of Crystallographic Data for Intermetallic Phases* (OSM, Metals Park, 1985).
- ²⁴A. Eichler, J. Hafner, and G. Kresse, *J. Phys.: Condens. Matter* **8**, 7659 (1996).
- ²⁵M. V. Ganduglia-Pirovano and M. Scheffler, *Phys. Rev. B* **59**, 15533 (1999).

- ²⁶A. F. Holleman and E. Wiberg, *Lehrbuch der Anorganischen Chemie* (Walter de Gruyter, Berlin, New York, 1995).
- ²⁷E. J. Walter, S. P. Lewis, and A. M. Rappe, *J. Chem. Phys.* **113**, 4388 (2000).
- ²⁸O. R. Inderwildi and A. Sundermann (private communication).
- ²⁹S. Schwegmann, H. Over, V. D. Renzi, and G. Ertl, *Surf. Sci.* **375**, 91 (1997).
- ³⁰R. A. v. Santen and M. Neurock, *Catal. Rev. - Sci. Eng.* **37**, 557 (1995).
- ³¹R. A. v. Santen, M. C. Zonneville, and A. P. J. Jansen, *Philos. Trans. R. Soc. London, Ser. A* **341**, 269 (1992).
- ³²X. Xu and C. M. Friend, *J. Am. Chem. Soc.* **113**, 6779 (1991).
- ³³G. S. Hammond, *J. Am. Chem. Soc.* **77**, 334 (1955).
- ³⁴O. R. Inderwildi, Q. Su, D. Lebedez, O. Deutschmann, and J. Warnatz (unpublished).